WJE

Cypress Avenue Over Murrells Inlet Creek (S-26-154) Bridge Rehabilitation

Substructure Evaluation

Cypress Avenue
Murrells Inlet, South Carolina 29576

WJE

Cypress Avenue Over Murrells Inlet Creek (S-26-154) Bridge Rehabilitation

Substructure Evaluation

Cypress Avenue
Murrells Inlet, South Carolina 29576

Michael C. Brown, PhD, PE, FACI
Associate Principal

Elizabeth Wagner, PhD, PE
Senior Associate

Trevor Moore, EIT
Associate II

CONTENTS

INTRODUCTION AND BACKGROUND

As part of Package 18 of the South Carolina Department of Transportation (SCDOT) On-Call Design-Build Support Engineering Services Contract No. 00232 (HNTB project number 77766), Wiss, Janney, Elstner Associates, Inc. (WJE) has performed an assessment of the 'Cypress Avenue Bridge', Bridge S-26-154 (Fed ID 9211) over the Murrells Inlet Creek near Murrells Inlet in Horry County, South Carolina. On-site work was performed September 26-28, 2023, followed by laboratory studies at WJE's laboratory facilities. WJE executed field inspections of the bridge substructure elements focused primarily on bent caps, performed testing to assess the development of corrosion, and collected field samples for assessment of the material condition of the concrete substructure. This report summarizes the field investigation, laboratory testing, and service life modeling for the bridge. The report conveys findings and conclusions along with recommendations relative to the feasibility for future reuse of the substructure elements. In developing recommendations, WJE considered the efficacy and benefit of applying appropriate cathodic protection to reach the desired service life.

DESCRIPTION OF STRUCTURE

The subject structure (Bridge S-26-154; Fed ID 9211) carries the eastbound and westbound lanes of Cypress Avenue over Murrells Inlet Creek. Murrells Inlet, to which the creek feeds, opens to the Atlantic Ocean and is a tidal water body. The bridge typically undergoes large daily wetting cycles, with tidal cycles exceeding five feet that alternately submerge and expose substructure bent caps and sections of the piles. The structure, built in 1997, consists of three continuous concrete slab spans, totaling 69 feet in length (Figure 1). The spans are supported by four bents, which are each comprised a cast-in-place reinforced concrete bent cap and either four prestressed concrete piles for the interior bents or five prestressed concrete piles for the end bents.

According to an August 2020 routine safety inspection report, the general condition rating for the structural deck (both deck and superstructure) was 3 (Serious) attributed to extensive corrosion of the underside of the flat slab. The substructure condition was reported to be 8 (very good). The August 2023 inspection report indicated deck/superstructure ratings of 3, with substructure rating of 7 (Good).
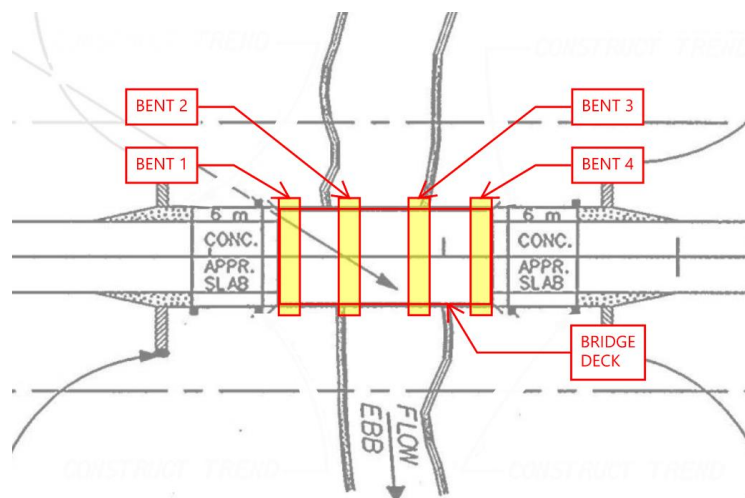

Figure 1. Overview of Cypress Ave bridge with labeled bent caps.

FIELD INVESTIGATION AND TESTING

WJE performed a field evaluation of the bridge substructure bent caps as permitted by access to the structure around tidal schedules and existing grade. End bent piles were completely buried below the mudline; interior bent piles were visible for brief periods of time during low tide and covered with organic growth. Evaluation of the piles was further constrained by the close configuration of prestressing strands, which made core sampling prohibitively difficult without risking damage to the strands. It is assumed that the quality and condition of the precast, prestressed concrete piles is better than that of the reinforced concrete bent caps because of the higher strength and lower w/c concrete used, and cyclic wetting from tidal fluctuations versus much of the piles that are continually immersed or below the mud line; thus, the condition of the bent caps was conservatively representative of the overall condition of the bents.

Field Evaluation Methods

This investigation included sounding and general visual assessment of accessible bent cap faces, and multiple detailed investigations using nondestructive testing techniques (NDT) that include ground penetrating radar (GPR), half-cell potential (HCP) testing, and linear polarization resistance (LPR) at select locations. The hands-on field investigation used GPR, HCP testing, and LPR testing to characterize the current condition at representative locations on the concrete caps of bents 1 through 4. Concrete core samples were collected at the detailed assessment locations for laboratory testing.

Visual Assessment

WJE inspected the exposed substructure faces of bent caps 1 through 4, removing organic material as required to permit inspection and testing. Faces of the elements were sounded with a hammer to detect delamination. The piles were observed but did not undergo detailed testing, as the bent cap was considered representative of the corrosion environment for the bents.

Ground Penetrating Radar

GPR using a Structure Scan Mini with a 1600 MHz antenna was used to nondestructively determine the spacing and cover depth of the outer layers of steel reinforcing bars at five locations on the concrete bent caps. Calibration of the scans was performed by drilling a $^5/_8$-inch diameter hole over one of the reinforcing steel bars located by the GPR unit and directly measuring the depth of reinforcing steel cover by a probe and tape measure. The physical measurements were compared to GPR scans at the same locations to calibrate the GPR responses accordingly. Variable cover depth can greatly influence corrosion

Figure 2. GPR inspection on cleaned face of bent cap 2.

resistance of a reinforced concrete system, with less cover depth leading to a shorter infiltration path for chlorides or aggressive chemicals and more rapid deterioration of the structure. Confirming reinforcement

configuration is also important to ensure structural capacity matches the intended design. A representative photograph of GPR data collection is shown in Figure 2.

Half-Cell Potential Testing

WJE performed HCP testing in general accordance with ASTM C876, *Standard Test Method for Corrosion Potentials of Uncoated Reinforcing Steel in Concrete*, at the same five locations tested with the GPR. The HCP surveys were performed by locally drilling to expose and establish an electrical connection to the reinforcement and placing a copper-copper sulfate (Cu-CuSO$_4$) reference electrode with a sponge containing conductive solution on the surface of the concrete with a high impedance voltmeter in line to complete the electrochemical circuit (Figure 3). Electrical potentials were measured using the voltmeter to the nearest millivolt in a grid pattern aligned with reinforcing steel locations identified by GPR. Testing was generally performed on a 7-foot by 2.5-foot grid on the exposed vertical faces of the bent caps. After testing was completed, the drilled holed openings that were used for the electrical connection and depth measurements were filled with a prepackaged, non-shrink concrete repair material.

Figure 3. HCP testing of bent cap 4, showing reference electrode (orange arrow) and connection to reinforcing steel (blue arrow.)

Linear Polarization Resistance Testing

LPR testing was performed using an LPR Handheld Meter manufactured by BAC Corrosion Control Ltd to determine instantaneous corrosion rate of the reinforcing steel in the concrete. The LPR test imparted known increments of external electrical direct current between the instrument probe and the reinforcing steel. The corresponding shifts in corrosion potential of the reinforcing steel from its equilibrium (open-circuit) potential are measured, and the ratio of this change in potential to the applied current was the polarization resistance. The corrosion rate, calculated from the inverse of the polarization resistance, was expressed as thickness loss versus time (mils per year, or mpy). Calculation of corrosion rate as a thickness loss with time was determined by the LPR meter using an estimated surface area of the reinforcement participating in the test, based on probe and nominal bar size.

Field Evaluation Findings

Visual Assessment

Hammer sounding did not indicate any delaminations or subsurface voids on the substructure. Assessment of the concrete deck was outside the scope of this report; however, it typically exhibited advanced deterioration from widespread spalling and exposed reinforcing steel due to corrosion, as shown in Figure 4.

Figure 4. Representative deterioration of existing bridge deck in orange box and good condition of bent cap 4 with piles below grade in red box.
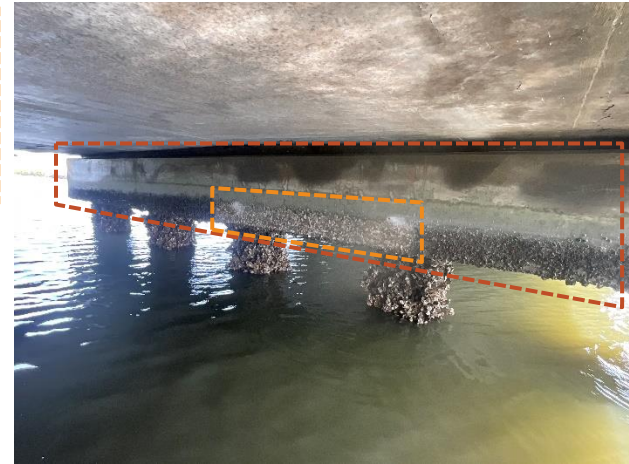

Figure 5. Good condition of concrete substructure at bent cap 3 in red. The representative region cleaned for inspection, HCP, and LPR testing is shown in orange.

The bent caps typically were in good condition, with minimal surface cracking, as shown in Figures 4 and 5. The condition of the end bent caps 1 and 4 matched the condition of the interior bent caps 2 and 3. There were no significant spalling or delamination observed on the substructure elements.

Narrow cracks were observed at locations near the bottom of the bent cap faces as shown in Figure 6. Corrosion byproduct (rust) were visible in-line with the bottom layer of longitudinal reinforcing in the bent cap. However, these occurrences were

Figure 6. Visible corrosion byproduct and cracking on bottom longitudinal reinforcing layer on bent cap 3.

localized and typically located only at the bottom layers of reinforcing steel. These are indicative of some degree of active corrosion, with the emergence of rust stains and limited cracking caused by the formation of the expansive corrosion byproducts.

Ground Penetrating Radar

The longitudinal and vertical spacing of reinforcing steel and cover depths in the bent caps were close to those detailed in the provided drawings, matching typically within an inch of tolerance of the design spacing. The reinforcing steel had an average cover depth of 2.3 inches (~58 mm) to the outer mat of longitudinal bars, which generally exceeded the design cover of 50 mm (~2 inches) indicated in drawings. However, on bent caps 1 and 3, GPR readings reflected cover depths less than the prescribed 50 mm. The minimum cover depth observed was 1.7 inches (~43 mm) on bent cap 1. The collected data are summarized in Table 1. The full data set is available in Table 1 of **Appendix A**.

Table 1. Summary table of GPR scan cover data

Bent	Cores	Vertical Bars		Longitudinal Bars	
		Average (in.)	Std. Dev. (in.)	Average (in.)	Std. Dev. (in.)
1	1, 2	1.90	0.14	2.23	0.56
2	3, 4	2.59	0.11	3.10	0.38
3	5, 6	2.29	0.34	2.91	0.52
4	7, 8	2.30	0.09	2.60	0.17
	Overall:	**2.28**	**0.32**	**2.85**	**0.53**

Half-Cell Potential Testing

Electrical potential contour maps based on the readings from the HCP testing were generated for the tested regions. Contour plots are provided in **Appendix B**, and an example contour plot is shown Figure 7. Per ASTM C876, HCP values more negative than -350 mV vs. a copper-copper sulfate electrode (CSE) can indicate a greater than 90% probability of active corrosion for reinforcing steel in concrete, as shown in Table 2. These guidelines are generally applicable for chloride-related corrosion in uncarbonated, atmospherically exposed elements. Note that carbonated concrete can exhibit a higher resistivity and show more positive potentials, whereas saturated concrete has a reduced resistivity and can therefore exhibit more negative potentials. As shown in Figure 7, and consistent through the contour plots in **Appendix B**, the measured HCP testing electrical potential values predominantly are more negative than -350 mV vs. CSE, indicating a very high probability of corrosion on the bent caps.
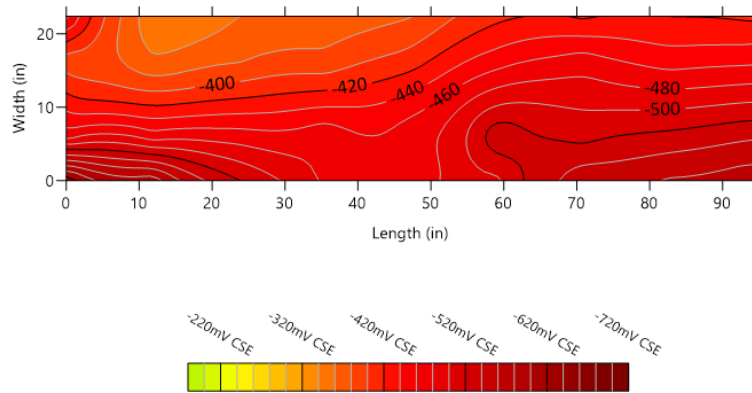

Figure 7. Representative electrical potential contour map from HCP test on bent cap 1.

Table 2. Levels of corrosion activity from half-cell potential electric potential measurements (ASTM C876)

Chloride-Driven Corrosion in Uncarbonated Concrete	
HCP (vs. CSE)	Corrosion Activity
> -200 mV	Low – 10% probability of corrosion
-200 to -350 mV	Moderate – increasing probability of corrosion
< -350 mV	High – 90% probability of corrosion

Note: HCP vs. CSE refers to HCP as measured using a copper–copper sulfate reference electrode (CSE).

Linear Polarization Resistance Testing

A minimum of two corrosion rate measurements were collected at each HCP testing region using the LPR meter. Results are summarized in Table 3. Categorizing the corrosion activity at the testing locations based on the categories shown in Table 4, there are high rates of corrosion at bent caps 1, 2 and 3. LPR results at bent 4 are comparatively low; it is possible that poor coupling of the device or high local concrete resistivity may have impacted the test results at this location. Overall, LPR testing active corrosion is occurring.

Table 3. LPR testing results

Bent cap	Corrosion Potential, E_{CORR} (mV CSE)	Corrected Corrosion Rate (mpy)	Qualitative Characterization of Corrosion Rate
1	-303	2.04	High
	-298	1.19	High
2	-346	2.32	High
	-302	1.50	High
	-419	2.54	High
3	-370	3.25	High
	-369	3.03	High
	-374	3.13	High
	-253	1.32	High
4	-746	0.05	Low
	-709	0.05	Low

Table 4. Levels of corrosion activity from corrosion rate measurements (ACI 228.2R-13)

Current Density (µA/cm²)	Thickness Loss (mm/year)	Thickness Loss (mpy)	Qualitative Characterization of Corrosion Rate
< 0.1	< 0.001	< 0.039	Negligible
0.1 to 0.5	0.001 to 0.005	0.039 to 0.20	Low
0.5 to 1.0	0.005 to 0.010	0.20 to 0.39	Moderate
> 1.0	> 0.010	> 0.39	High

Source: ACI 228.2R-13, *Report on Nondestructuve Test Methods for Evaluation of Concrete in Structures, Table 3.5.4.3*

Concrete Cores

WJE extracted a total of eight concrete cores comprised of one 4-inch diameter core and one 2.5-inch diameter core from each of four bent caps as summarized in Table 5. Cores were collected in general accordance with ASTM C42, *Standard Test Method for Obtaining and Testing Drilled Cores and Sawed Beams of Concrete.* A representative photograph of collection is shown in Figure 8.

After coring, the core holes were patched with a prepackaged, non-shrink concrete repair material (*Euclid Euco Repair V100 Overhead and Vertical Mortar)* approved by the SCDOT *Qualified Rapid Patch Materials for Concrete Pavement.*[1]

Figure 8. Bent cap 3 core extraction.

The core samples were packaged and shipped to WJE's laboratory testing facilities at the Janney Technical Center (JTC) in Northbrook, Illinois for testing. As summarized in Table 5, the 4-inch diameter cores (Cores 1, 3, 5, and 7) were intended for both petrographic analysis and chloride profile analysis, while the 2.5-inch cores (Cores 2, 4, 6, and 8) were used for chloride profile analysis.

WJE also collected two water samples at opposite bridge abutments, from the southern ends of bents 1 and 4, as summarized in Table 6. WJE packaged and shipped these samples to the JTC for testing.

---

[1] South Carolina Department of Transportation, *Qualified Rapid Patch Materials for Concrete Pavement*, September 8, 2023. http://info2.scdot.org/Materials/QualProd/22%20QPL.pdf.

Table 5. Concrete core testing matrix

Core ID	Bent cap	HCP Test	Core Diameter (inch)	Date Collected	Laboratory Test Methods
1	1	-	4	9/28/2023	Petrography & Chloride Profiles
2	1	E1	2.5	9/28/2023	Chloride Profiles
3	2	-	4	9/27/2023	Petrography & Chloride Profiles
4	2	E2	2.5	9/27/2023	Chloride Profiles
5	3	-	4	9/27/2023	Petrography & Chloride Profiles
6	3	-	2.5	9/27/2023	Chloride Profiles
7	4	E5	4	9/27/2023	Petrography & Chloride Profiles
8	4	-	2.5	9/27/2023	Chloride Profiles

Table 6. Water sample testing matrix

Sample ID	Bent	Date Collected	Laboratory Test Method
S1-9/28/23	1	9/28/2023	pH, Chloride Content & Total Dissolved Solids
S2-9/28/231	4	9/28/2023	pH, Chloride Content & Total Dissolved Solids

LABORATORY STUDIES

Petrographic Examinations

Petrographic studies were completed on cores 1, 3, 5, and 7 in accordance with the methods and procedures outlined in ASTM C856, *Standard Practice for Petrographic Examination of Hardened Concrete*. A nominal 1-inch-thick slab was cut longitudinally using a water-cooled continuous-rim diamond saw blade. One of the resulting surfaces of each slab was lapped to achieve a fine matte finish suitable for examination with a stereomicroscope. Lapping exposes textural features such that the edges of air voids, cracks, and aggregate constituents can be more easily observed. Fresh fracture surfaces were also prepared to study the physical characteristics of the concrete. Lapped and fracture surfaces were examined using a stereomicroscope (5 to 63 times magnification) equipped with a digital camera. Lapped sections surfaces are shown in Figure D5 through Figure D8 in **Appendix D**. A thin section was prepared from the exterior region of the remaining surface facing the lapped sections from each core. The thin sections were examined at magnifications ranging from 25× to 500× using a petrographic (polarized-light) microscope.

General Concrete Characterization

The following observations pertain to each of the examined cores, unless otherwise stated.

- The cores did not contain macrocracking or embedded steel. Images of each core in its as-received condition are shown in Figures D1 through Figure D4 in **Appendix D**.

- The cores for petrographic examination were partial depth cores, 3-3/4 inches in diameter, and ranged in length from 4-1/2 to 5-1/4 inches long.

- The concrete represented by each of the examined cores contained similar constituents in relatively similar proportions, and likely represent the same or very similar concrete mixtures.

- The exterior surfaces were formed and did not exhibit distress (cracking, spalling) except around the core perimeter from core removal.

- The concretes are composed of crushed siliceous coarse aggregate and natural siliceous sand fine aggregate dispersed within an air entrained portland cement paste.

Aggregate

The coarse aggregate was composed of angular to subrounded crushed siliceous aggregate. The nominal maximum aggregate size within each core was 1/2-inch, but Core 7 also had a visually higher volume of 1/4-inch or finer coarse aggregate particles (Figure D6 and Figure D8, **Appendix D**). The aggregate was composed of felsite.

The fine aggregate was composed of natural siliceous sand, which was comprised of predominantly quartz with lesser amounts of feldspar and mica. Some of the aggregate particles (quartz/quartzite, felsite) were considered potentially susceptible to alkali silica reaction (ASR). Isolated occurrences of ASR were observed in cores 1 and 5, with cracking and ASR gel emanating from reactive particles into the surrounding paste and air voids. Portions of cores 1 and 5 were placed in a sealed bag with damp paper towels for 2 days to promote ASR growth; no additional ASR growth was observed. No large-scale distress or deterioration away from the isolated occurrences of ASR were observed. Reactive particles were isolated, and no interconnected microcracks were observed in the cores. The aggregate was uniformly distributed and generally well graded in each of the examined cores.

Paste

The paste in each of the examined cores was a light to medium gray. The paste contained portland cement, with no visually detected supplementary cementitious materials such as fly ash or slag cement (Figure D10, **Appendix D**). The cement grains were well hydrated, although a higher volume of residual cement was observed in the exterior nominal 1 mm of each core. A moderate volume of calcium hydroxide cement hydration product (portlandite) was observed in the bulk of the paste. Intermittent, isolated regions of paste that appeared leached of calcium were observed within the top surface region of cores 3, 5, and 7, which measured up to 1 mm in core 5 and less than 1 mm in cores 3 and 7 (Figure D11, **Appendix D**). Otherwise, portlandite crystals were evenly dispersed throughout non-carbonated areas of paste. A thin (less than 1 mm) "crust" of calcite was intermittently observed on the exterior surfaces of cores 3, 5, and 7 (Figure D12, **Appendix D**). Carbonation was localized and negligible (less than 1 mm or not observed) in cores 1, 3, and 7, and up to 1 mm in core 5 (Figures D9 and D11, **Appendix D**). The exterior surface of each core was uneven and rough.

On laboratory-induced fresh fracture surfaces, the paste had a vitreous to subvitreous luster, hackly to microgranular texture, was moderately absorptive to water, and was hard (could not be scratched with a

Mohs hardness pick of 3). Paste-to-aggregate bond was judged to be moderately strong, with fractures propagating predominantly through, but sometimes around, aggregate particles. Based on the observed features, estimated w/c of the cores was moderate to moderately low in a range from 0.40 to 0.45.

Air

The examined concrete was marginally air entrained. Entrained voids were spherical and ranged in size from very fine to coarse (Figure D13, **Appendix D**). Entrained air voids were generally well distributed throughout the paste, although accumulations of air voids and voids lining coarse aggregate particles were infrequently observed (Figure D14, **Appendix D**). Infrequent larger, irregularly shaped entrapped air voids were observed in each of the cores. Estimated air content ranged from 3 to 5 percent. Entrained air voids frequently contained deposits of secondary ettringite (Figure D15, **Appendix D**). Infrequent voids also contained ASR gel as discussed above (Figure D16, **Appendix D**).

Cracking

Infrequent surface-perpendicular microcracks were observed propagating from the exterior surface of each core. Microcracks were typically shallow (less than 1/4 inch into the concrete) and did not contain secondary deposits. Carbonation was slightly deeper along the microcracks. These microcracks may represent shrinkage cracks and are superficial and do not represent distress from a deterioration mechanism.

A slightly wider microcrack was observed in core 5, which propagated up to approximately 2 inches into the concrete. The crack propagated predominantly around, but sometimes through, aggregate particles and contained secondary deposits of ettringite and isolated occurrences of ASR gel (Figure D17, **Appendix D**). The crack also contained calcite deposits near the exterior surface. The particle from which the gel was emanating was not observed, so it cannot be concluded whether the crack was caused by the formation and expansion of ASR gel, or whether the crack had previously existed, and gel filled in the available space as it formed. Nevertheless, the gel is isolated, and the crack and ASR were not judged to be detrimental to the concrete.

Carbonation Examinations

Carbonation results in a decrease in pH of the concrete substructure and the corresponding degradation of the passivation layer on the reinforcing steel, leading to a higher risk of corrosion. The depth of carbonation from the exterior surface was assessed on the remaining portion of each core immediately after saw-cuttinng for petrographic examination and prior to saw-cutting for chloride profiling. The cut face of each core was allowed to dry, then immediately sprayed with pH-indicating phenolphthalein solution. The solution imparted a bright pink color on uncarbonated paste and remained colorless on carbonated paste. The sprayed portions of the cores were then used for chloride ion content analysis.

The depths of carbonation in cores 1, 3, 5, and 7 were found to be negligible, as shown in representative Figures 9 and 10 for cores 3 and 5, respectively. The limited carbonation in the cores assessed for carbonation indicates that there is likely little contribution from carbonation in promoting reinforcing steel corrosion at this time.
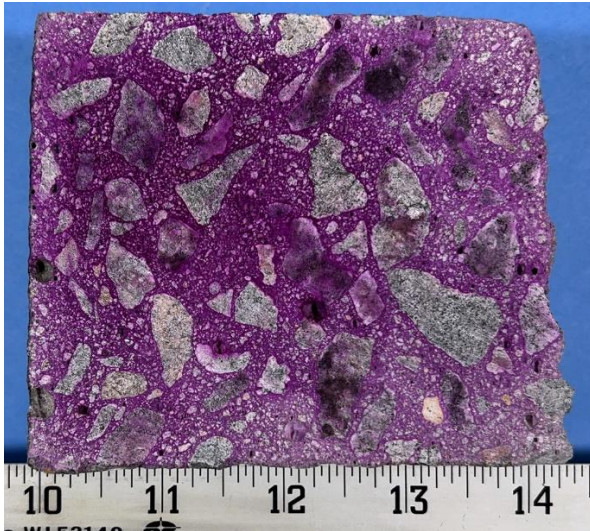
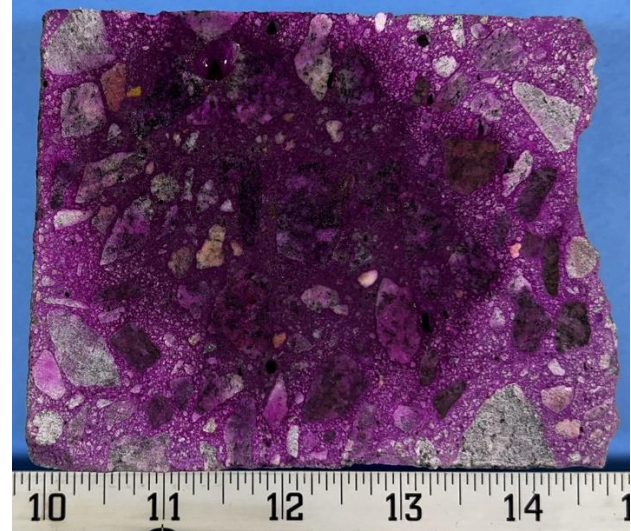Figure 9. Core 3 carbonation test – no carbonation visible

Figure 10. Core 5 carbonation test – no carbonation visible

Chloride Profile Analysis

Chloride profile analysis was performed on cores 1 through 8 to evaluate chloride concentrations versus depth relative to the surface of the bent caps. For this testing, the cores were saw-cut into ¼-inch slices at defined depths near the surface, near the bar, and at ranges above and below the bar to characterize variation with depth. The slices were finely ground for chloride extraction and measurement. Acid-soluble chloride testing was performed in accordance with ASTM C1152, *Standard Test Method for Acid-Soluble Chloride in Mortar and Concrete.* The acid-soluble chloride concentratoin is the combination of both the free and chemically bound chloride within the concrete. This method provides an upper bound for the concentration of chlorides that could potentially contribute to corrosion of reinforcement The results of this testing are summarized in Figures 11, 12, 13, and 14, and the associated table of chloride concentration data by depth is provided in Table 1 of **Appendix C**. The results support the strong likelihood of active corrosion, as the chloride concentrations at the depths of reinforcing steel in concrete bent caps 2, 3, and 4 exceed a nominal chloride concentration threshold of 0.05 percent by weight of concrete (500 ppm)[2], or approximately 1.9 lb/yd³ of concrete. This is the concentration at which the passivation of reinforcing steel begins to break down and corrosion may begin. Furthermore, most chloride concentrations at the depths of reinforcing steel in bent caps 2, 3, and 4 exceed the chloride concentration of 0.10 percent by weight of concrete, which has a 'very high' probability of corrosion, as summarized in Table 7.
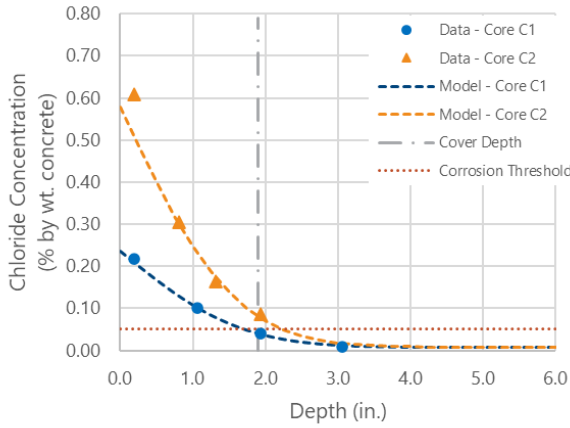

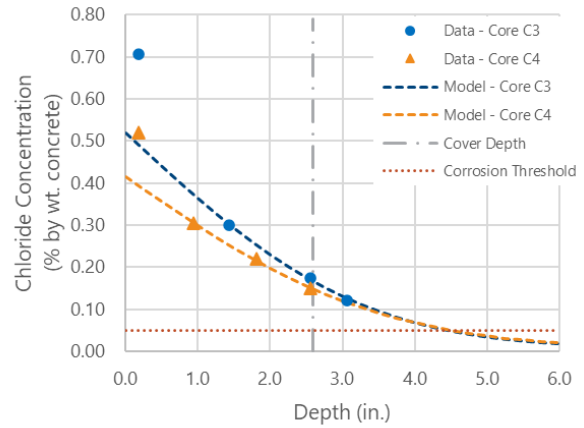Figure 11. Chloride concentration vs. depth – bent cap 1

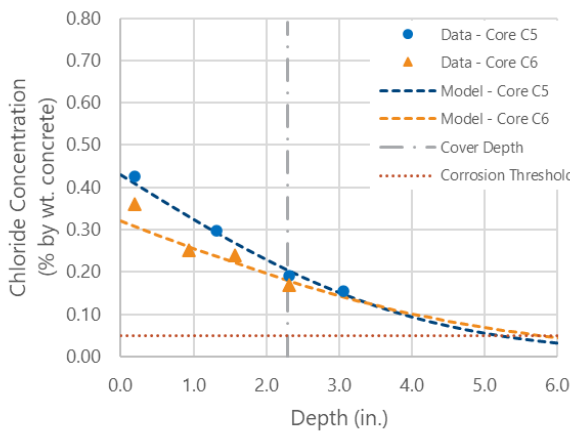Figure 12. Chloride concentration vs. depth – bent cap 2

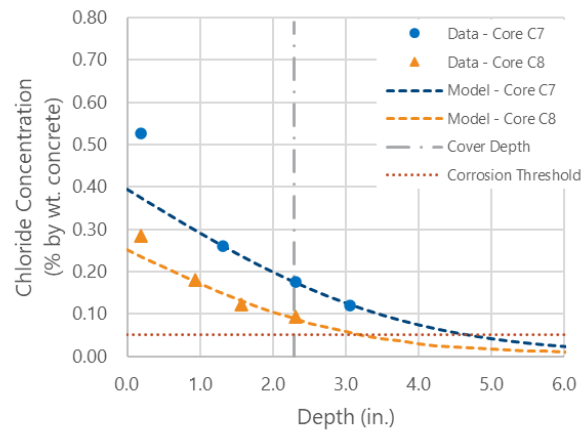Figure 13. Chloride concentration vs. depth – bent cap 3

Figure 14. Chloride concentration vs. depth – bent cap 4

Table 7. Corrosion "risk" for uncoated carbon-steel (ASTM A615) reinforcement bars

% Chloride by Weight of Concrete	Probability of Corrosion Initiation	"Risk" Category
<0.03	<1%	Negligible
0.03 to 0.04	1 to 10%	Low
0.04 to 0.07	10 to 50%	Moderate
0.07 to 0.10	50 to 90%	High
>0.10	>90%	Very High

Source: Adapted from (Broomfield 2007)[3], based on data from (Breit 1997)[4]

---

[3] Broomfield, John P. 2007. Corrosion of Steel in Concrete. New York: Taylor and Francis.

[4] Breit, W. (1997). Untersuchungen zum kritischen korrosionsauslösenden Chloridgehalt für Stahl in Beton (Dissertation In German). Schriftenreihe Aachener Beiträge zur Bauforschung.

Water Sample Analysis

The two water samples were analyzed for pH, chloride content, and total dissolved solids. Testing for the pH was determined in accordance with ASTM E70, *Standard Test Method for pH of Aqueous Solutions with the Glass Electrode.* The chloride content was determined in accordance with ASTM D512, *Standard Test Method for Chloride Ion in water.* Total dissolved solids were determined by evaporation. The results of the water sample testing are shown in Table 8.

Table 8. Water testing results

Sample	S1-9/28/23	S2-9/28/23
pH	7.09	6.99
Chloride Content (ppm)	11,590	2,106
Total Dissolved Solids (ppm)	21,000	23,720

The tested pH, chloride content, and total dissolved solids are in line with expectations for a brackish marine environment subject to tidal variations (Table 9). Chloride content in S1 is nearly 5 times that of S2, despite samples being taken approximately 50 feet apart.

Table 9. Approximate values for pH, chloride, and total dissolved solids in natural water bodies

Classification	pH	Chloride (ppm)	Total dissolved solids (ppm)
Pure water	7	0	0
Fresh water	6	1-500	<1,000
Brackish water	7-8	1000-10,000	1,000-10,000
Salt water	8	>10,000	>10,000
Sea water	8	35,000	>35,000

Adapted from C, Lamont-Doherty Earth Observatory. 2011. Chloride and Salinity. New York, NY: Columbia University.

SERVICE LIFE MODELING

In consideration of the variability inherent in concrete elements, a probabilistic service life model was employed using WJE Corrosion and Service Life Evaluation (CASLE) to estimate the amount of active corrosion in the outer reinforcing bars and the amount of corrosion-related deterioration in the bent caps expected over time due to chloride exposures. WJE CASLE models the ingress of chloride ions through concrete based on Fick's Second Law of Diffusion. The rate at which chloride ions move from the surface of an element through the concrete is characterized by the concrete's apparent diffusion coefficient. When the concentration of chloride ions at the depth of the reinforcing steel exceeds a critical threshold concentration, corrosion is likely to initiate. Over time, the build-up of corrosion products on the surface of the reinforcing bars can lead to subsequent cracking, delamination, and surface damage to the element. The time between corrosion initiation and the time at which surface damage occurs is called the propagation time.

The probabilistic modeling approach adopted by WJE CASLE for existing structures recognizes that corrosion is a local process that can develop at multiple locations on a single element over time. The model predicts the amount of an element's surface area affected by corrosion initiation or corrosion-related damage as a function of time, based on statistical distributions of key input parameters that are considered to govern corrosion, such as the surface chloride concentration, the apparent diffusion coefficient of the concrete, and the cover over the reinforcing steel. Statistical distributions for each parameter are determined based on the data collected in the field and laboratory studies. A Monte Carlo simulation is performed in which the surface is essentially subdivided into several thousand elements, each having exposures, chloride transport properties, and cover depths that are sampled from the statistical distributions for each parameter. The time at which the chloride concentration exceeds the critical threshold at the depth of the reinforcing steel (i.e., the time-to-corrosion initiation) is determined for each instance, and the result is presented as the percentage of the element surface predicted to exhibit active corrosion or corrosion-related damage as a function of time.

Model Inputs

The input parameters into the service life model can be separated into exposures and resistances to corrosion initiation. Exposure parameters include the ambient temperature and the chloride concentration at the surface of the element and its rate of build-up at that surface over time. Resistance parameters include the concrete cover to the reinforcing steel, the apparent diffusion coefficient of the concrete as a function of time, and the critical chloride threshold of the reinforcing steel. The propagation time between corrosion initiation and surface damage was assumed to be equal to 10 years, although this parameter can vary depending on the quality, electrical resistivity, and degree of saturation of the concrete.

The chloride exposure and apparent diffusion coefficient of the concrete were estimated based on model fits to the acid-soluble chloride ion concentration profiles shown in Figure 11Figures 11 through 14. A model fit was performed for each core to determine the chloride exposure concentration and 28-day apparent diffusion coefficient of the concrete that resulted in a chloride profile that most closely aligned with the measured profile. The model fitting assumed that the chloride concentration at the surface of the element builds up to its maximum concentration over a period of 1 year from time of construction and that the diffusion coefficient decreases over time according to an exponential function as follows:

$$D(t) = D_{28} \left(\frac{28 \text{ days}}{t} \right)^{m}$$

where D_{28} is the 28-day apparent diffusion coefficient and m is an aging exponent assumed to be equal to 0.20 for concrete not containing supplementary cementitious materials (SCMs).

The model fits are shown in Figures 11 through 14, and the fitted 28-day apparent diffusion coefficient (D_{28}) and surface chloride concentration (C_s) are summarized in Table 10. For service life modeling of the four bent caps, the surface chloride exposure concentration was assumed to vary according to a normal distribution with a mean equal to 3850 ppm by mass of concrete and a standard deviation of 1155 ppm by mass of concrete, consistent with the average and standard deviation calculated from the eight cores. The D_{28} for each bent cap was also modeled as a normal distribution with an assumed mean equal to the average D_{28} estimated for each pair of cores, with the exception of bent cap 3, for which the mean D_{28} was assumed to equal the value estimated for core 5 only. The apparent diffusion coefficient estimated for core 6 is comparable to values typically measured at or near cracks and may suggest that chloride ingress

at that location is influenced by mechanisms other than diffusion. The standard deviation for the apparent diffusion coefficient was based on an assumed coefficient of variation of 40%, which is consistent with the coefficient of variation among cores sampled from bent caps 2, 3, and 4.

Table 10. Surface chloride concentrations (C_s) and 28-day apparent diffusion coefficients (D_{28}) based on fitted chloride profiles

Core	Fitted D_{28} (in^2/yr)	Fitted C_s (ppm by mass of concrete)
Bent Cap 1 – Core 1	0.09	2280
Bent Cap 1 – Core 2	0.09	5700
Bent Cap 2 – Core 3	0.36	5110
Bent Cap 2 – Core 4	0.42	4070
Bent Cap 3 – Core 5	0.54	4220
Bent Cap 3 – Core 6	0.81	3120
Bent Cap 4 – Core 7	0.47	3860
Bent Cap 4 – Core 8	0.31	2440
Average	**0.38**	**3850**
Coefficient of Variation	**62%**	**31%**

The statistical distributions of concrete cover were based on the measured cover to the longitudinal reinforcing bars for each bent cap. Cover was assumed to vary according to a normal distribution with a mean and standard deviation equal to the values shown in Table 1. For bent caps 1, 2, and 4, the measured standard deviation was less than 1/8 inch, so a larger standard deviation of 1/4 inch was assumed for these cases to reflect more typical variation during construction.

The chloride threshold of the reinforcing steel was assumed to follow the distribution described in

Table 7, which reflects a beta distribution with a mean of 0.48% by mass of cement, a standard deviation of 0.15% by mass of cement, and lower and upper limits of 0.2% and 2.0% by mass of cement, respectively.[5] Conversion from percent by mass of cement to parts per million (ppm) by mass of concrete was based on an assumed cementitious materials content of 564 pounds per cubic yard of concrete and a unit weight of 145 pounds per cubic foot of concrete.

The model input parameters assumed for each bent cap are summarized in Table 11.

---

[5] Breit, W. (1997). *Untersuchungen zum kritischen korrosionsauslösenden Chloridgehalt für Stahl in* Beton (Dissertation In German). Schriftenreihe Aachener Beiträge zur Bauforschung.

Table 11. Summary of model input parameters

Parameter	Probability Distribution	Value[1]			
		Bent Cap 1	Bent Cap 2	Bent Cap 3	Bent Cap 4
Average Ambient Temperature (°F)	Deterministic	m = 64.4	m = 64.4	m = 64.4	m = 64.4
Surface Chloride Concentration, Cs (ppm)	Normal	m = 3850 s = 1155	m = 3850 s = 1155	m = 3850 s = 1155	m = 3850 s = 1155
Build-up Time (yr)	Deterministic	m = 1	m = 1	m = 1	m = 1
28-day Apparent Diffusion Coefficient (in^2/yr)	Normal	m = 0.09 s = 0.04	m = 0.39 s = 0.16	m = 0.54 s = 0.22	m = 0.39 s = 0.16
Aging Factor, m (--)	Deterministic	m = 0.20	m = 0.20	m = 0.20	m = 0.20
Cover depth (in.)	Normal	m = 1.90 s = 0.25	m = 2.59 s = 0.25	m = 2.29 s = 0.34	m = 2.30 s = 0.25
Chloride Threshold (ppm)	Beta	m = 691 s = 216 LL = 288 UL = 2881	m = 691 s = 216 LL = 288 UL = 2881	m = 691 s = 216 LL = 288 UL = 2881	m = 691 s = 216 LL = 288 UL = 2881
Propagation Time (yr)	Deterministic	m = 10	m = 10	m = 10	m = 10

[1]: m = mean; s = standard deviation; LL = lower limit; UL = upper limit

Model Results and Discussion

Results of the service life model are summarized in Table 12. The model predicts that 37 percent of the outer reinforcing steel in bent cap 1 is actively corroding and more than 80 percent of the outer reinforcing steel in the other three bent caps is actively corroding. These predictions are generally supported by the high chloride ion concentrations measured within the eight cores and the highly negative half-cell potentials measured in these locations.

The model also predicts that 16 percent of the surface of bent cap 1 and more than 60 percent of the surfaces of the other three bent caps are currently experiencing damage due to chloride-induced corrosion. These predictions are greater than the amounts of corrosion damage observed during WJE's field studies and may suggest a longer propagation time than the 10-year propagation period assumed by the models. The occurrence of surface damage due to corrosion is a function of the concrete's tensile strength and the corrosion rate of the reinforcing steel, which itself is a function of temperature, moisture and oxygen exposure. While damage has not manifested at the levels predicted by the corrosion modeling, chloride concentrations are currently high enough to initiate widespread corrosion within the bent caps and damage associated with this corrosion is likely to occur if the corrosion is not mitigated.

Table 12. Predicted percent corrosion initiation and damage

Bent Cap	Predicted % Corrosion Initiation (2023)	Predicted % Corrosion Damage (2023, 10-year propagation time)
Bent Cap 1	37%	16%
Bent Cap 2	81%	63%
Bent Cap 3	91%	84%
Bent Cap 4	88%	77%

CONCLUSIONS AND RECOMMENDATIONS

The detailed HCP and LPR testing indicate a high likelihood of active corrosion in the bent caps, which is further supported by the high chloride ion concentrations measured in core samples and the findings from the service life modeling performed. The high chloride content of the water typically surrounding the bridge and the continued tidal action provide ample exposure to aggressive chlorides in service. Service life modeling predicts greater degrees of corrosion-induced damage than are currently observed on the bents. The difference may be attributed in part to the high degree of saturation of the concrete, which can limit the availability of oxygen to feed the cathodic reaction in the corrosion cell. Such occurrence would be characterized by high degrees of chloride contamination and high electrical potentials, but comparatively low corrosion rates and therefore slower initiation of damage. Once corrosion progresses to the point of crack initiation, a path is opened for oxygen ingress and the rate of corrosion can be expected to exponentially increase. It appears the bents are just reaching this point based on observed rust product near the bottom faces of caps.

Despite the high probability of active corrosion occurring in the bent caps, the concrete substructure is still currently in overall good condition, as verified through hands-on visual inspection. Petrographic evaluation showed limited effects of carbonation, and no significant evidence of deleterious internal chemical formations, aggressive exterior chemical attack, or other factors leading to material distress. Therefore, chloride-induced corrosion appears to be the largest risk to the continued use of the concrete substructure. Service life modeling predicts greater degrees of corrosion-induced damage than are currently observed on the bents. Without intervention, active corrosion is expected to degrade the concrete structure at an accelerating rate – reducing performance of the structure through section loss of reinforcing steel, as well as concrete deterioration through spalling and cracking with the formation of expansive rust.

Since manifest cracking, delamination and spalling are not present, there is an opportune window to mitigate the corrosion before significant damage occurs. It is recommended that a galvanic (or passive) cathodic protection system be installed on the exposed bridge substructure. A properly designed cathodic system would be expected to sufficiently slow the rate of corrosion reaction through consumption of a sacrificial anode to achieve the desired additional service life for this structure, deferring replacement of the structure. Application of marine-rated, surface mounted bulk anodes below the waterline, exterior galvanic jackets on prestressed concrete piles, and a network of anodes embedded in the bent caps that are all tied to the existing reinforcing steel could protect the embedded reinforcement for 20 to 25 years.

Additional investigation of specific conditions may be required to develop detailed repair drawings, and engineer oversight of repair installation is recommended.

Our conclusions are based on a review of available documents, field observations and testing at the time of our investigation. Other conditions may exist or develop over time that were not found during the site visit or identified during the development of this report. The repair recommendations provided are conceptual and associated estimates of probable cost are subject to change as repair strategies become more refined, quantities or severity increase in magnitude due to worsening conditions, or material and labor costs fluctuate due to market conditions.

CLOSING

We appreciate the opportunity to assist HNTB with this important project for SCDOT. Please contact us if we can provide additional assistance.

APPENDIX A. GROUND PENETRATING RADAR RESULTS

Concrete cover depths measured by GPR are presented herein.

Table A1. Table of calibrated GPR scan cover depths

Bent Cap	Cover Depth (inch)	Reinforcing Steel Orientation
1	1.67	Vertical
1	1.83	Vertical
1	1.83	Vertical
1	1.75	Vertical
1	1.91	Vertical
1	1.91	Vertical
1	2.06	Vertical
1	2.06	Vertical
1	2.06	Vertical
1	2.54	Longitudinal
1	2.77	Longitudinal
1	2.13	Longitudinal
1	1.50	Longitudinal
2	2.43	Vertical
2	2.60	Vertical
2	2.77	Vertical
2	2.68	Vertical
2	2.77	Vertical
2	2.52	Vertical
2	2.52	Vertical
2	2.52	Vertical
2	2.60	Vertical
2	2.52	Vertical
2	3.27	Longitudinal
2	3.27	Longitudinal
2	3.43	Longitudinal
2	3.27	Longitudinal
2	3.35	Longitudinal
2	3.02	Longitudinal
2	2.93	Longitudinal
2	2.25	Longitudinal
3	2.66	Vertical
3	2.71	Vertical
3	2.66	Vertical
3	2.46	Vertical
3	2.62	Vertical
3	2.66	Vertical

Bent Cap	Cover Depth (inch)	Reinforcing Steel Orientation
3	2.66	Vertical
3	2.66	Vertical
3	3.25	Longitudinal
3	3.17	Longitudinal
3	3.72	Longitudinal
3	3.67	Longitudinal
3	3.42	Longitudinal
3	3.42	Longitudinal
3	2.46	Longitudinal
3	2.29	Longitudinal
3	2.46	Longitudinal
3	2.12	Vertical
3	2.03	Vertical
3	1.95	Vertical
3	1.87	Vertical
3	1.95	Vertical
3	1.95	Vertical
3	1.95	Vertical
3	2.03	Vertical
3	2.03	Vertical
3	3.04	Longitudinal
3	2.71	Longitudinal
3	2.12	Longitudinal
3	2.37	Longitudinal
3	2.75	Longitudinal
3	2.75	Longitudinal
4	2.15	Vertical
4	2.19	Vertical
4	2.31	Vertical
4	2.35	Vertical
4	2.23	Vertical
4	2.35	Vertical
4	2.27	Vertical
4	2.35	Vertical
4	2.44	Vertical
4	2.72	Longitudinal
4	2.48	Longitudinal

APPENDIX B. HALF-CELL POTENTIAL RESULTS

Contour plots of HCP tests in general accordance with ASTM C876, *Standard Test Method for Corrosion Potentials of Uncoated Reinforcing Steel in Concrete* are presented herein.

WJE

Wiss, Janney, Elstner Associates, Inc.
2941 Fairview Park Drive, Suite 300
Falls Church, Virginia 22042
703.641.4601 tel
www.wje.com

Half-Cell Potential Survey
Cypress Avenue Bridge (S-26-154)
Test E1, Bent Cap 1
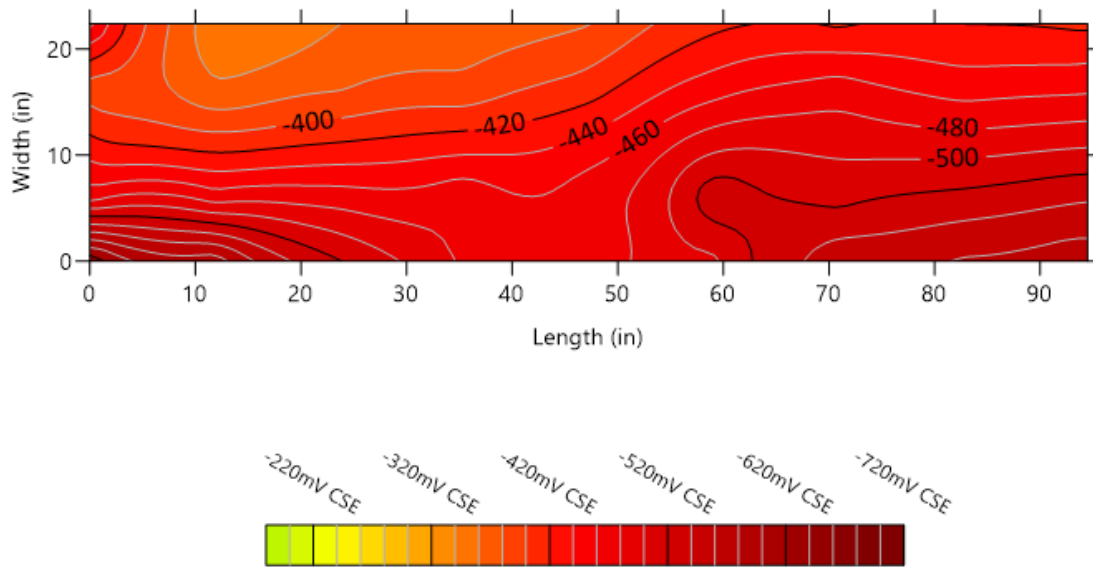
Surveyed by: MCB/THM
Date: September 26, 2023

Per ASTM C876-15 Appendix X.1:

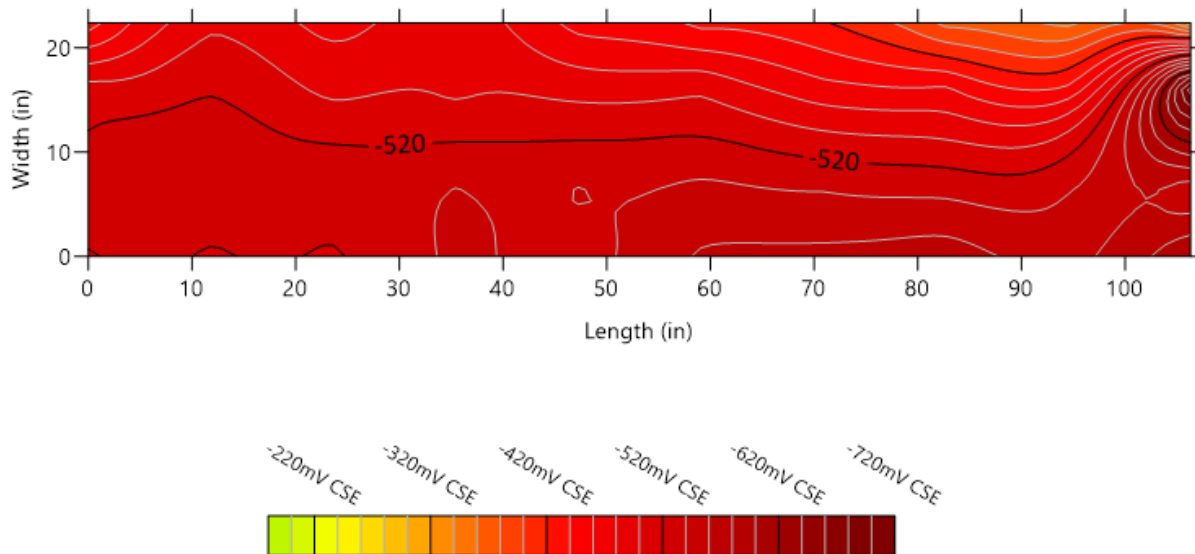|	
x ≥ -200 mV CSE	> 90% probability of no corrosion at time of test
-200 > x ≥ -350 mV	CSE Corrosion activity is uncertain
x < -350 mV CSE	> 90% probability of corrosion at time of test

Figure B1. Bent cap 1 HCP testing per ASTM C876

WJE

Half-Cell Potential Survey
Cypress Avenue Bridge (S-26-154)
Test E2, Bent Cap 2
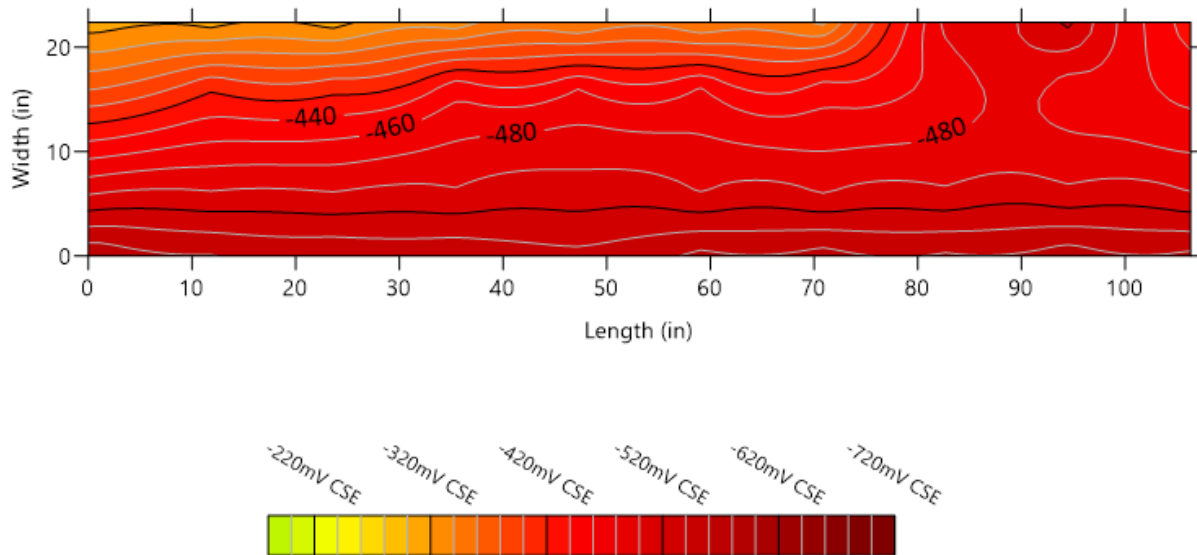
Surveyed by: MCB/THM
Date: September 26, 2023

Per ASTM C876-15 Appendix X.1:

x ≥ -200 mV CSE	> 90% probability of no corrosion at time of test
-200 > x ≥ -350 mV CSE	Corrosion activity is uncertain
x < -350 mV CSE	> 90% probability of corrosion at time of test

Figure B2. Bent cap 2 HCP testing per ASTM C876

WJE

Wiss, Janney, Elstner Associates, Inc.
2941 Fairview Park Drive, Suite 300
Falls Church, Virginia 22042
703.641.4601 tel
www.wje.com

Half-Cell Potential Survey
Cypress Avenue Bridge (S-26-154)
Test E3, Bent Cap 3
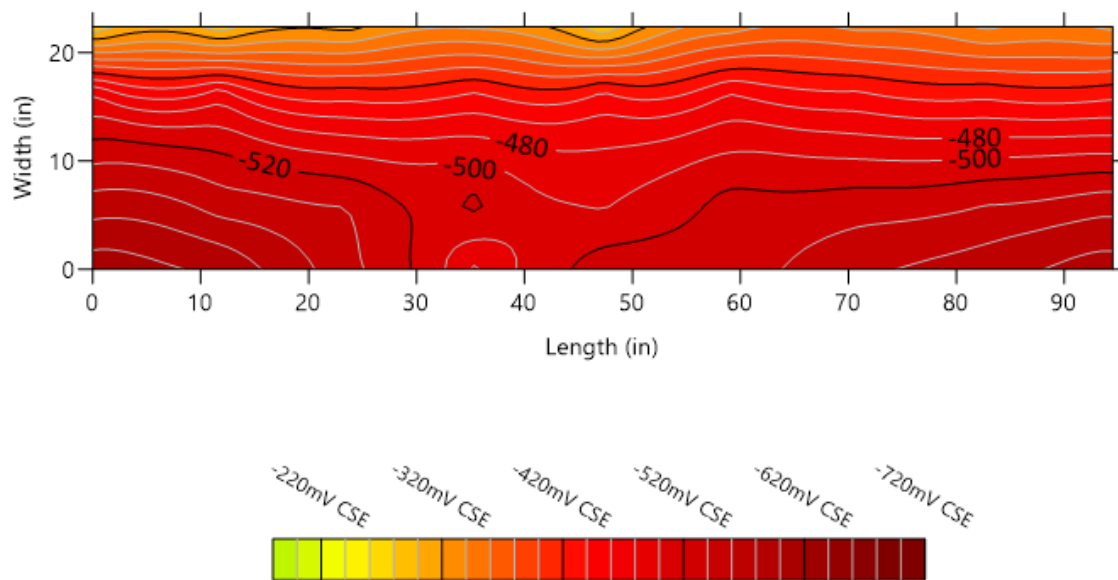
Surveyed by: MCB/THM
Date: September 26, 2023

Per ASTM C876-15 Appendix X.1:

x ≥ -200 mV CSE	> 90% probability of no corrosion at time of test
-200 > x ≥ -350 mV CSE	Corrosion activity is uncertain
x < -350 mV CSE	> 90% probability of corrosion at time of test

Figure B3. Bent cap 3 HCP testing per ASTM C876

WJE

Half-Cell Potential Survey
Cypress Avenue Bridge (S-26-154)
Test E4, Bent Cap 3
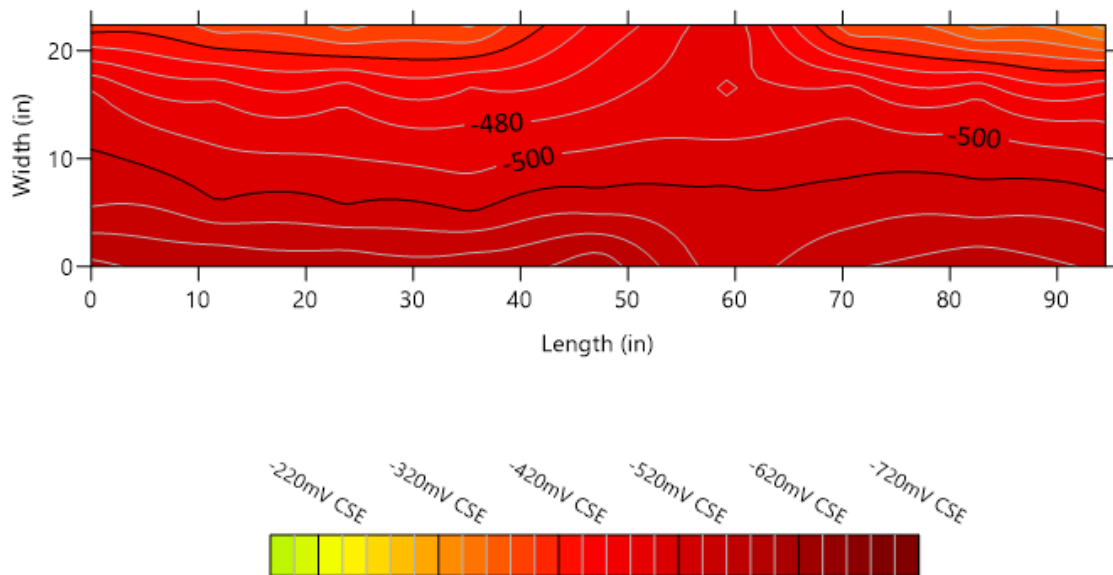
Surveyed by: MCB/THM
Date: September 26, 2023

Per ASTM C876-15 Appendix X.1:

x ≥ -200 mV CSE	> 90% probability of no corrosion at time of test
-200 > x ≥ -350 mV	CSE Corrosion activity is uncertain
x < -350 mV CSE	> 90% probability of corrosion at time of test

Figure B4. Bent cap 3 HCP testing per ASTM C876

Wiss, Janney, Elstner Associates, Inc.
2941 Fairview Park Drive, Suite 300
Falls Church, Virginia 22042
703.641.4601 tel
www.wje.com

Half-Cell Potential Survey
Cypress Avenue Bridge (S-26-154)
Test E5, Bent Cap 4

Surveyed by: MCB/THM
Date: September 26, 2023

Per ASTM C876-15 Appendix X.1:

x ≥ -200 mV CSE	> 90% probability of no corrosion at time of test
-200 > x ≥ -350 mV CSE	Corrosion activity is uncertain
x < -350 mV CSE	> 90% probability of corrosion at time of test

Figure B5. Bent cap 4 HCP testing per ASTM C876

APPENDIX C. CHLORIDE CONCENTRATION TESTING

Results of concrete chloride concentration tests are presented herein.

Table C1. Acid-soluble chloride contents of concrete core slices collected in accordance with ASTM C1152, *Standard Test Method for Acid-Soluble Chloride in Mortar and Concrete*

Core ID	Slice Designation	Slice Depth from Core Surface (inch)	Acid-Soluble Chloride, % by mass of sample
1	A	$1/8$ - $1/4$	0.218
	B	NT	NT
	C	1 - $1\,1/8$	0.102
	D	$1\,7/8$ - 2	0.041
	E	3 - $3\,1/8$	0.008
2	A	$1/8$ - $1/4$	0.609
	B	$3/4$ - $7/8$	0.305
	C	$1\,1/4 - 1\,3/8$	0.164
	D	$1\,7/8$ - 2	0.087
	E	NT	NT
3	A	$1/8$ - $1/4$	0.706
	B	NT	NT
	C	$1\,3/8$ - $1\,1/2$	0.3
	D	$2\,1/2 - 2\,5/8$	0.173
	E	3 - $3\,1/8$	0.122
4	A	$1/8$ - $1/4$	0.52
	B	$7/8$ - 1	0.305
	C	$1\,3/4$ - $1\,7/8$	0.219
	D	$2\,1/2 - 2\,5/8$	0.149
	E	NT	NT
5	A	$1/8$ - $1/4$	0.427
	B	NT	NT
	C	$1\,1/4 - 1\,3/8$	0.297
	D	$2\,1/4 - 2\,3/8$	0.192
	E	3 - $3\,1/8$	0.155
6	A	$1/8$ - $1/4$	0.36
	B	$7/8$ - 1	0.251
	C	$1\,1/2 - 1\,5/8$	0.24
	D	$2\,1/4 - 2\,3/8$	0.17
	E	NT	NT
7	A	$1/8$ - $1/4$	0.526
	B	NT	NT
	C	$1\,1/4 - 1\,3/8$	0.26
	D	$2\,1/4 - 2\,3/8$	0.176
	E	3 - $3\,1/8$	0.121

Red coloring indicates 'very high' probability of corrosion initiation. NT indicates the slice was not tested.

Core ID	Slice Designation	Slice Depth from Core Surface (inch)	Acid-Soluble Chloride, % by mass of sample
8	A	$^1/_8$ - $^1/_4$	0.285
	B	$^7/_8$ - 1	0.181
	C	$1^1/_2 - 1^5/_8$	0.122
	D	$2^1/_4 - 2^3/_8$	0.094
	E	NT	NT

Red coloring indicates 'very high' probability of corrosion initiation. NT indicates the slice was not tested.

APPENDIX D. PETROGRAPHIC EXAMINATION FIGURES

Representative images of concrete samples as analyzed in general accordance with ASTM C876, *Standard Test Method for Corrosion Potentials of Uncoated Reinforcing Steel in Concrete* are presented herein.

Figure D1. Core 1. Images of the sample as-received, with the exterior surface in the exterior left image, bottom surface in the exterior right image, and longitudinal view of the core with the exterior surface facing left in the bottom image.
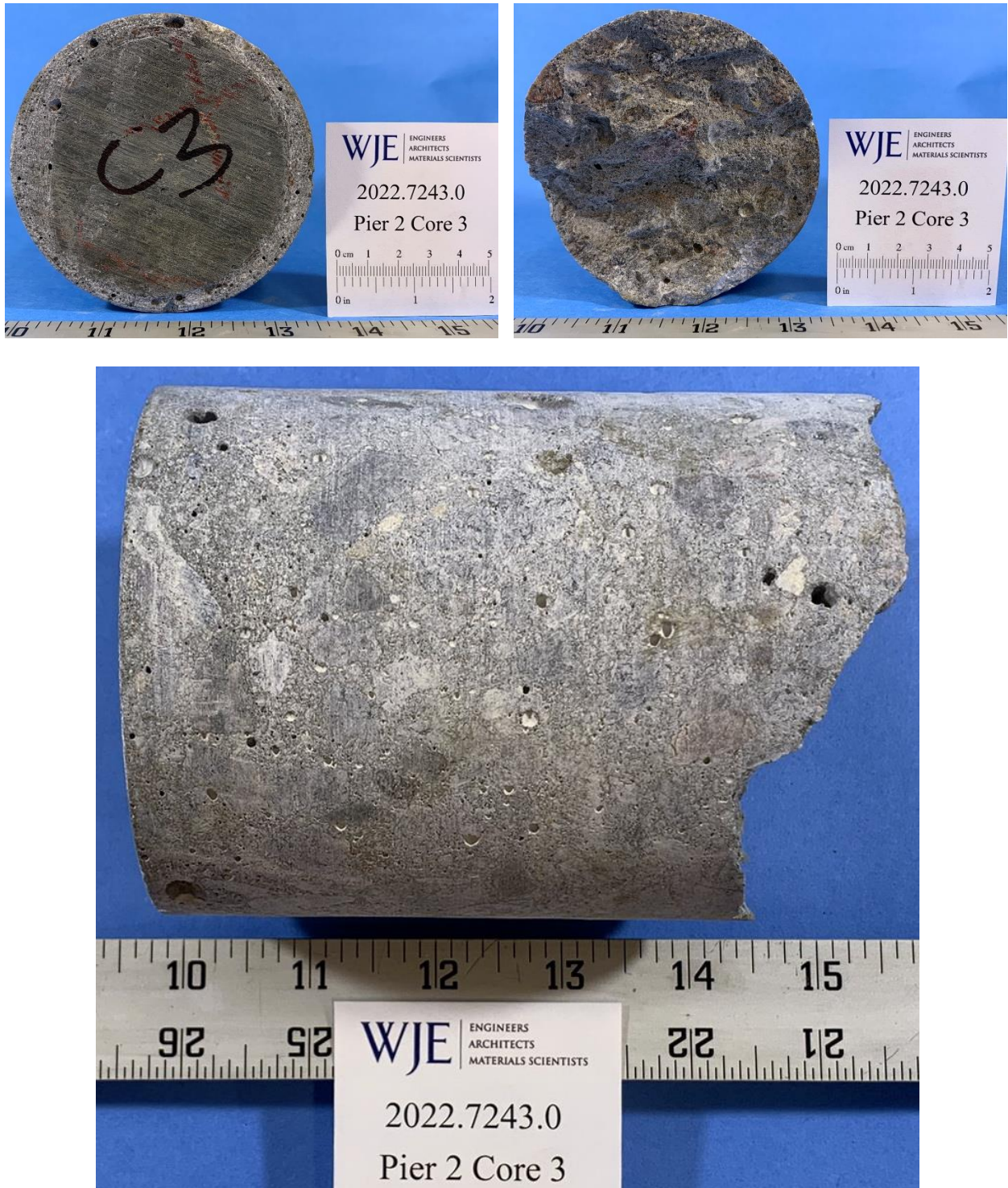
Figure D2. Core 3. Images of the sample as-received, with the exterior surface in the exterior left image, bottom surface in the exterior right image, and longitudinal view of the core with the exterior surface facing left in the bottom image.
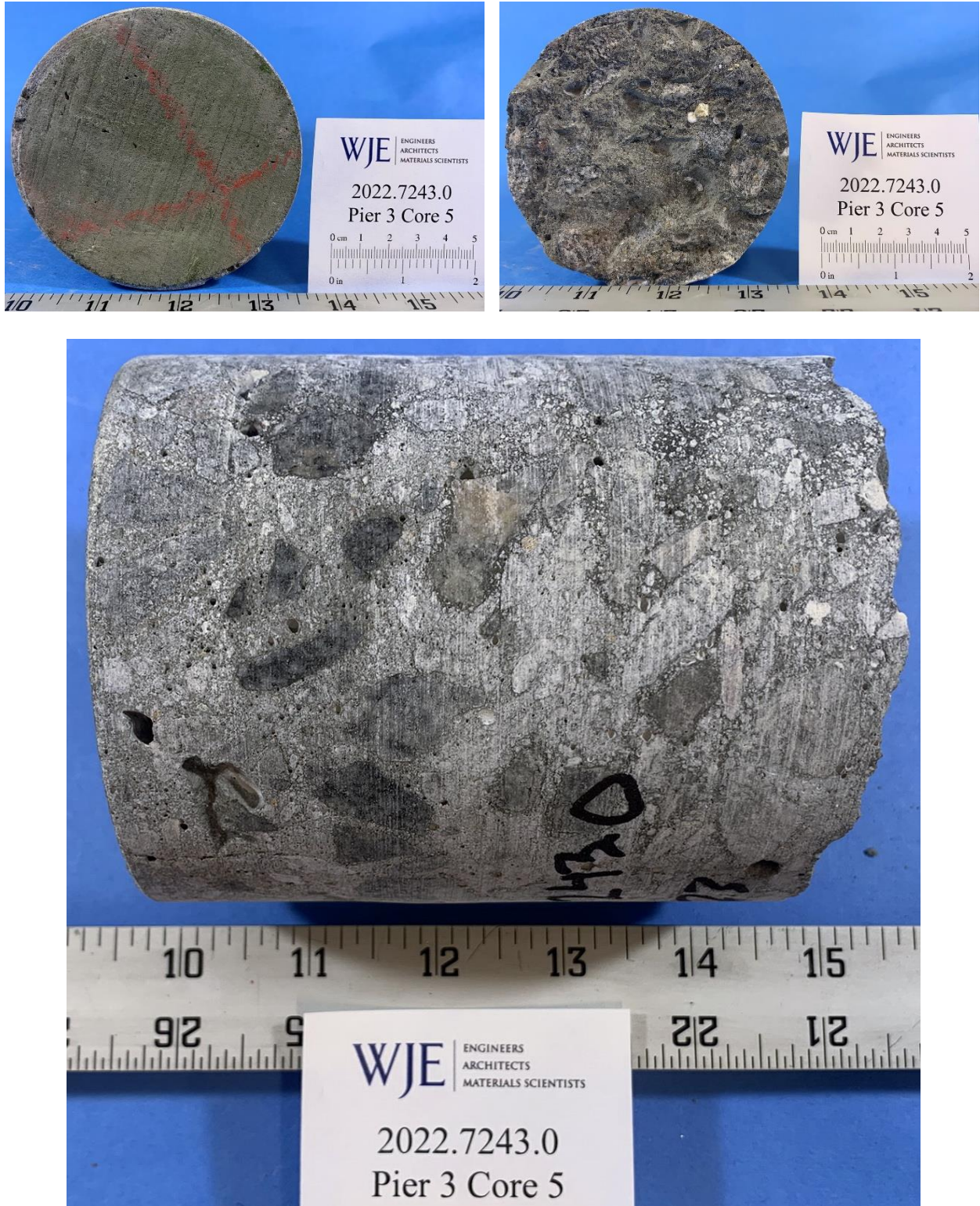
Figure D3. Core 5. Images of the sample as-received, with the exterior surface in the exterior left image, bottom surface in the exterior right image, and longitudinal view of the core with the exterior surface facing left in the bottom image.
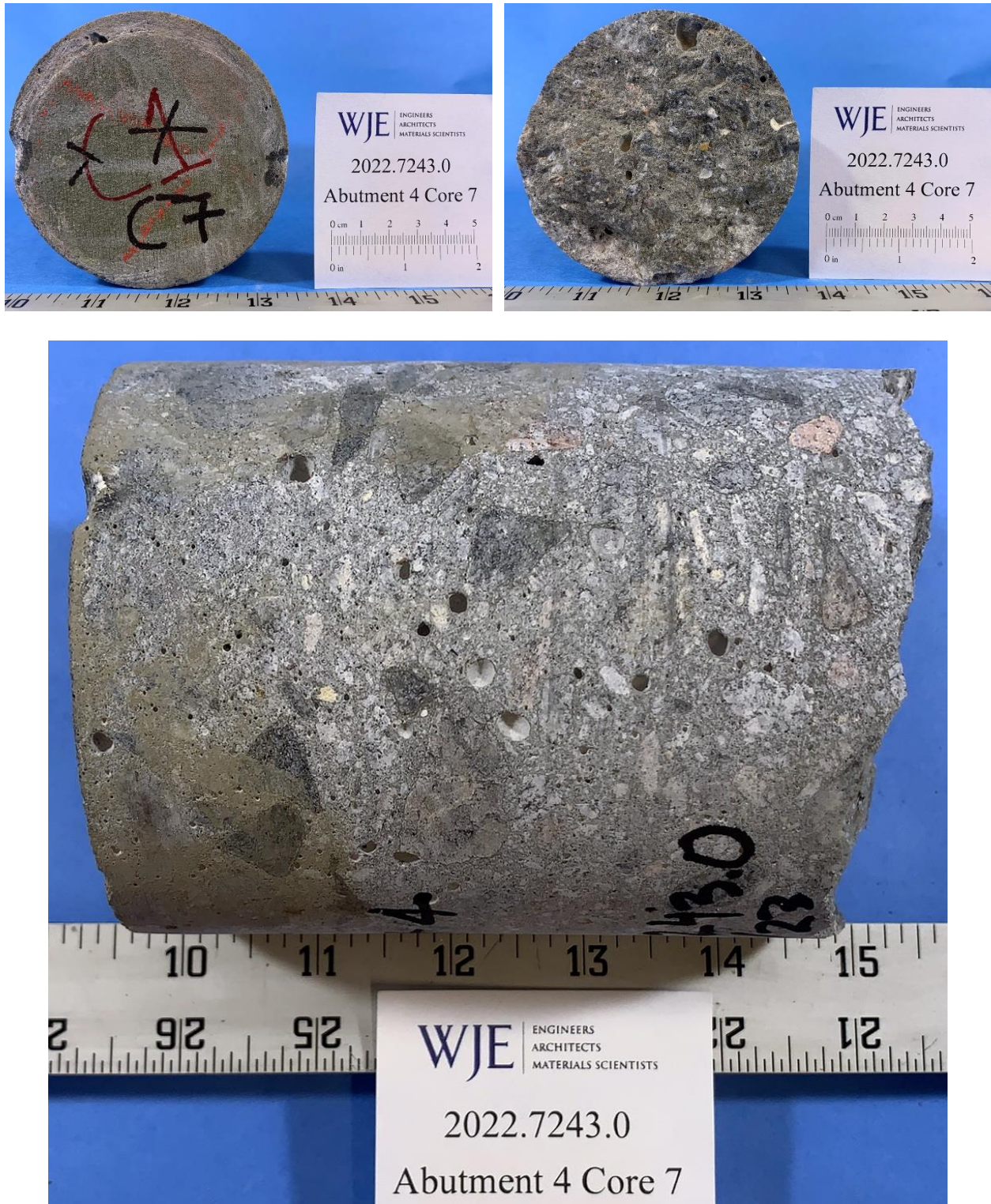
Figure D4. Core 7. Images of the sample as-received, with the exterior surface in the exterior left image, bottom surface in the exterior right image, and longitudinal view of the core with the exterior surface facing left in the bottom image.
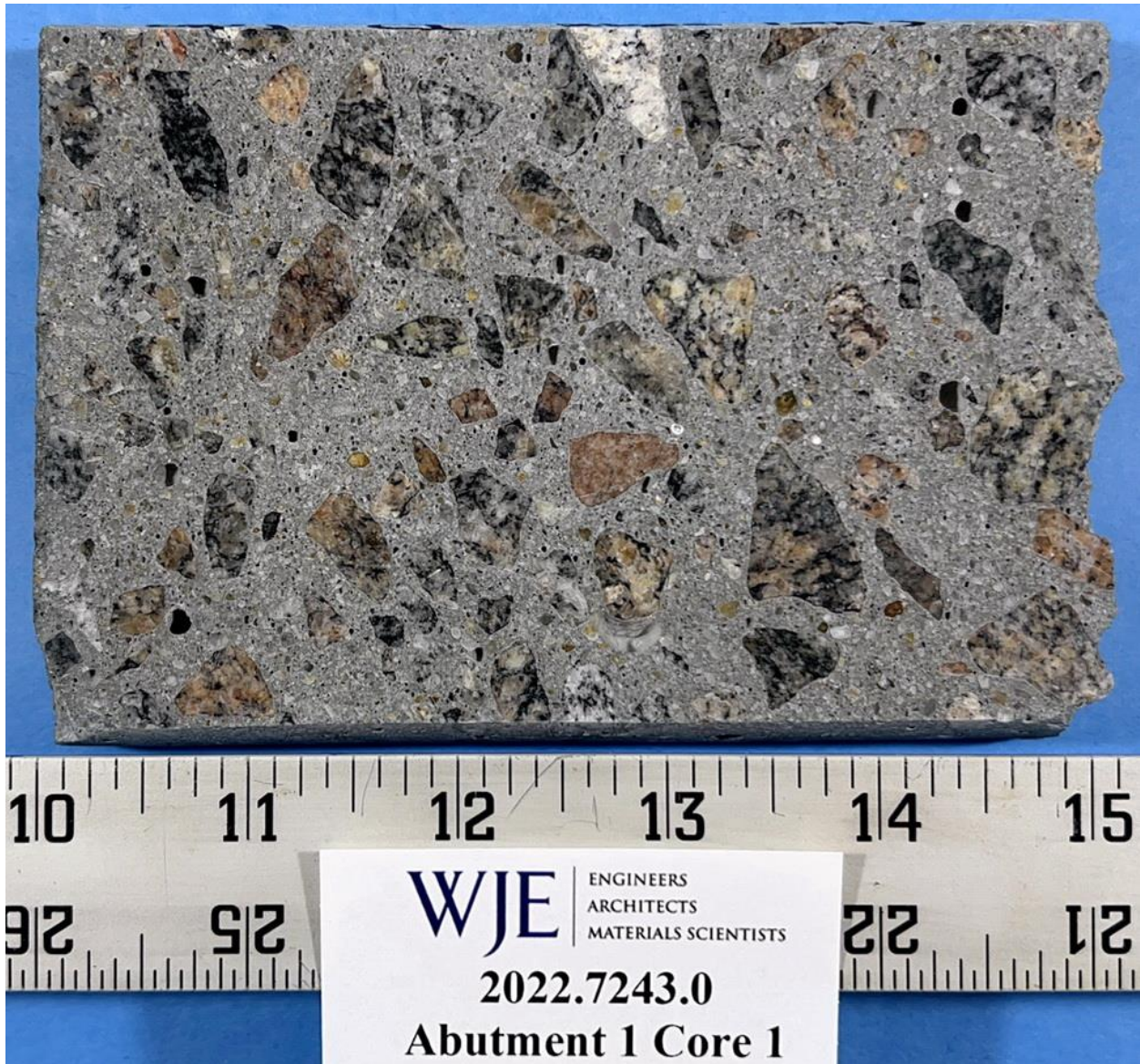
Figure D5. Core 1. Lapped cross section, with the exterior surface facing left.
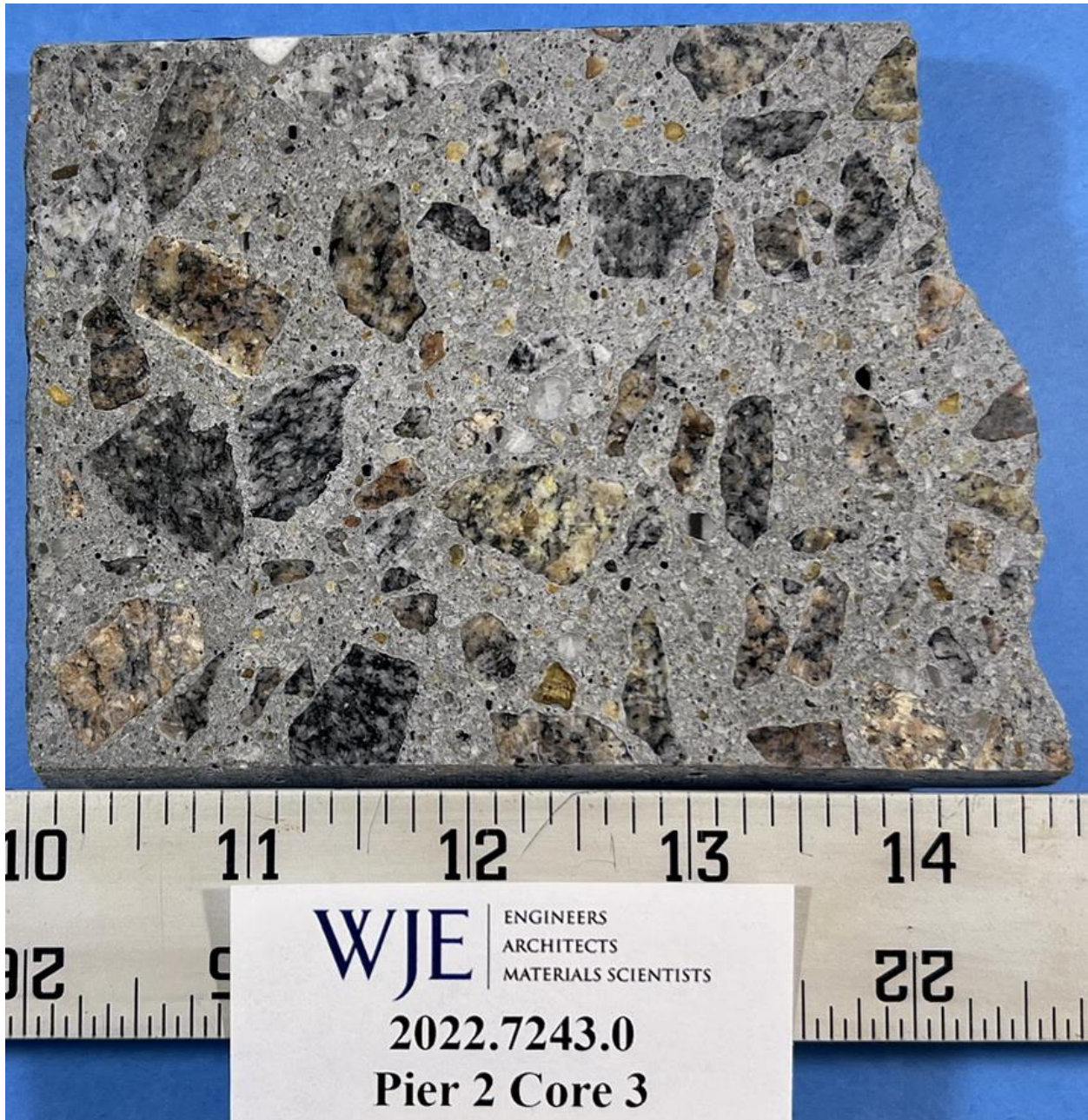
Figure D6. Core 3. Lapped cross section, with the exterior surface facing left.

Figure D7. Core 5. Lapped cross section, with the exterior surface facing left.

Figure D8. Core 7. Lapped longitudinal cross section, with the exterior surface facing left. Note the generally smaller coarse aggregate compared to the other three cores.

Figure D9. Core 7. Cut longitudinal face shortly after being sprayed with phenolphthalein solution. Note that the entire surface is pink, indicating no carbonation of the paste. None of the tested cores showed carbonation.
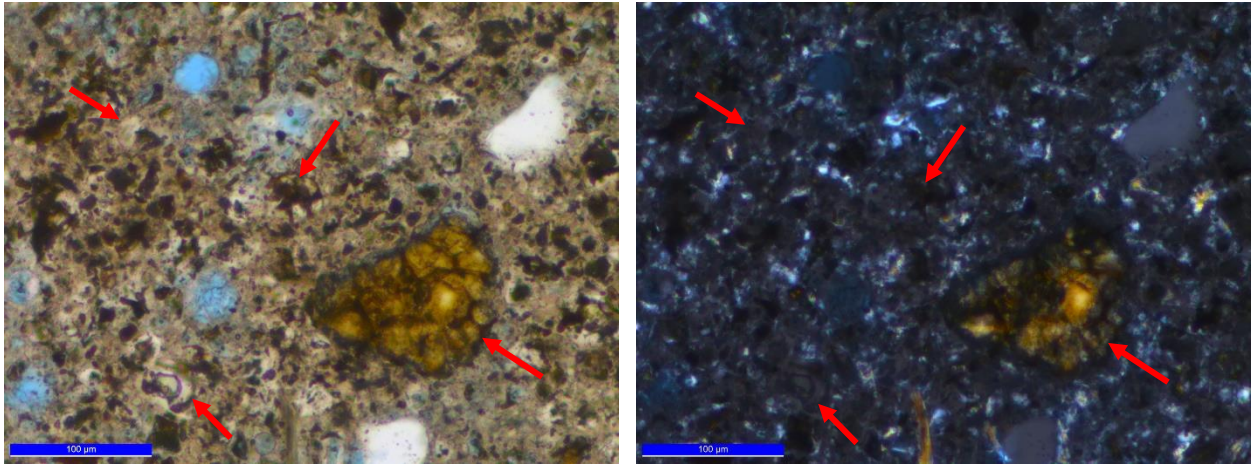
Figure D10. Core 3. Representative area of paste showing portland cement particles (red arrows). Left image taken in plane-polarized light, right image taken in cross-polarized light.
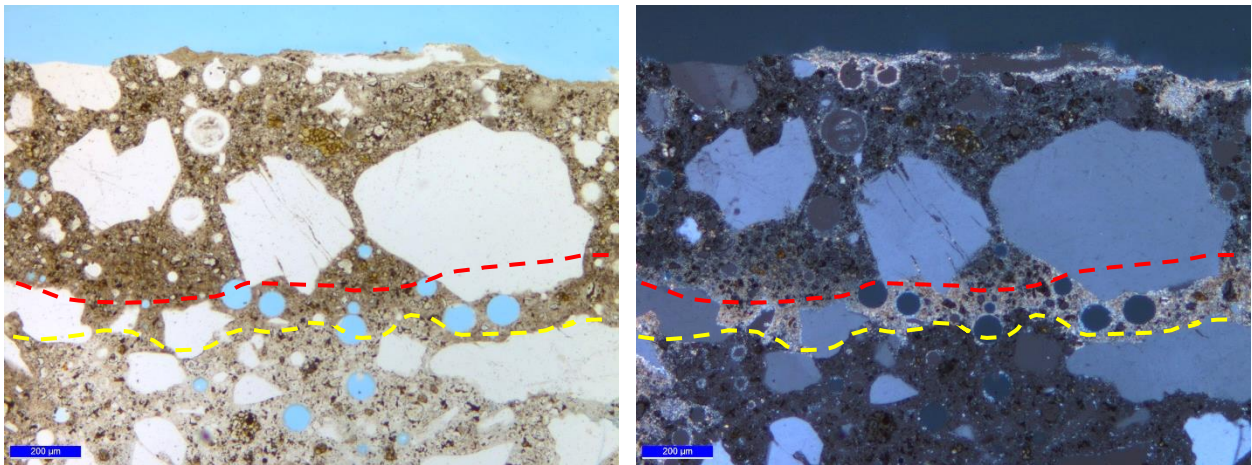
Figure D11. Exterior surface region of Core 5, showing calcium leaching within the exterior nominal 500 mils (1/2 inch, above the red dashed line), and carbonated paste just below the leached zone (between the red and yellow dashed lines). Left image taken in plane-polarized light, right image taken in cross-polarized light.
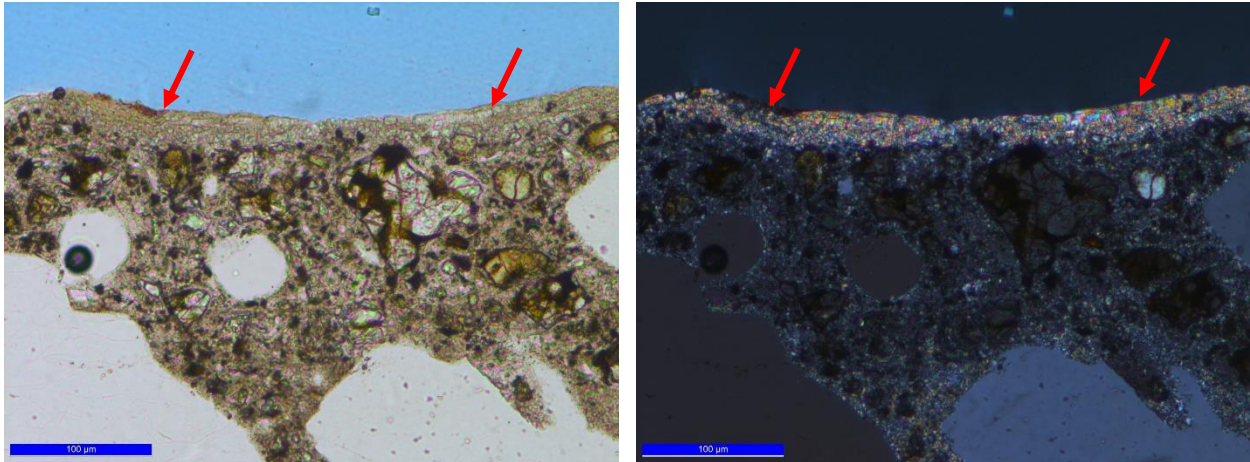
Figure D12. Core 3. Thin calcite crust along the exterior surface of the core (red arrows). The crust is localized, across the core surface but is continuous in this field of view. Left image taken in plane-polarized light, right image taken in cross-polarized light.
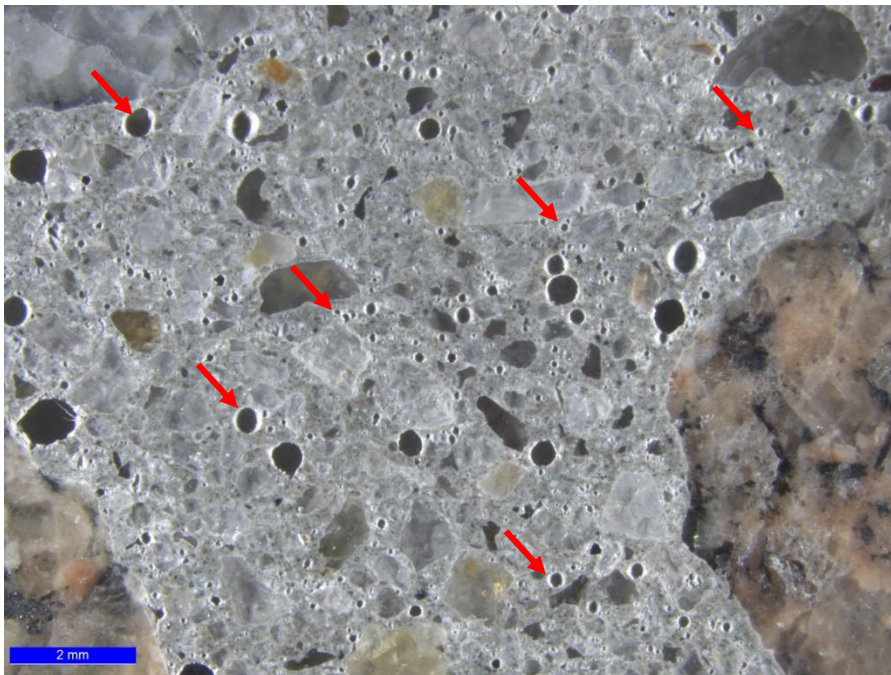
Figure D13. Core 5. Representative area of the concrete showing the typical air system. Note that voids are typically spherical in shape and range in size from very fine to coarse. Red arrows indicate select voids.
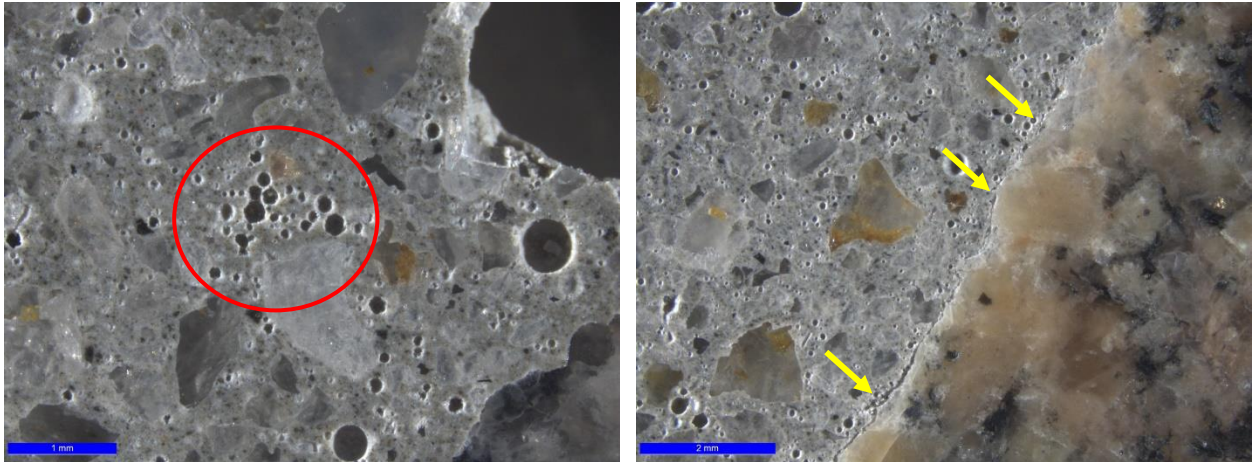
Figure D14. Core 3. Entrained air void accumulations (left image, within red circle) and entrained air voids and a microcrack lining a coarse aggregate particle (right image, yellow arrows).
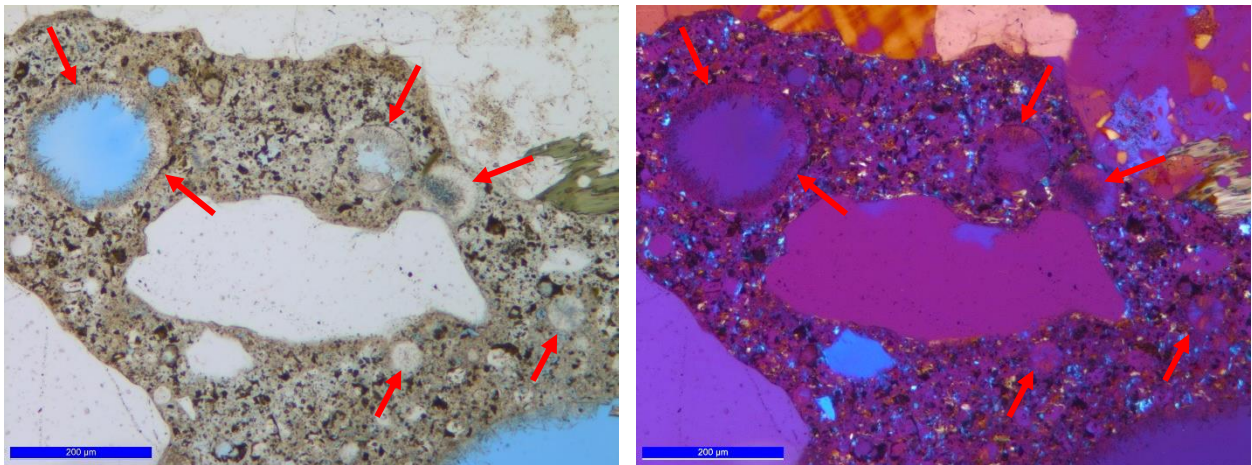
Figure D15. Core 7. Secondary deposits of ettringite were observed lining entrained air voids (red arrows). Left image taken in plane-polarized light, right image taken in cross-polarized light with a gypsum plate.
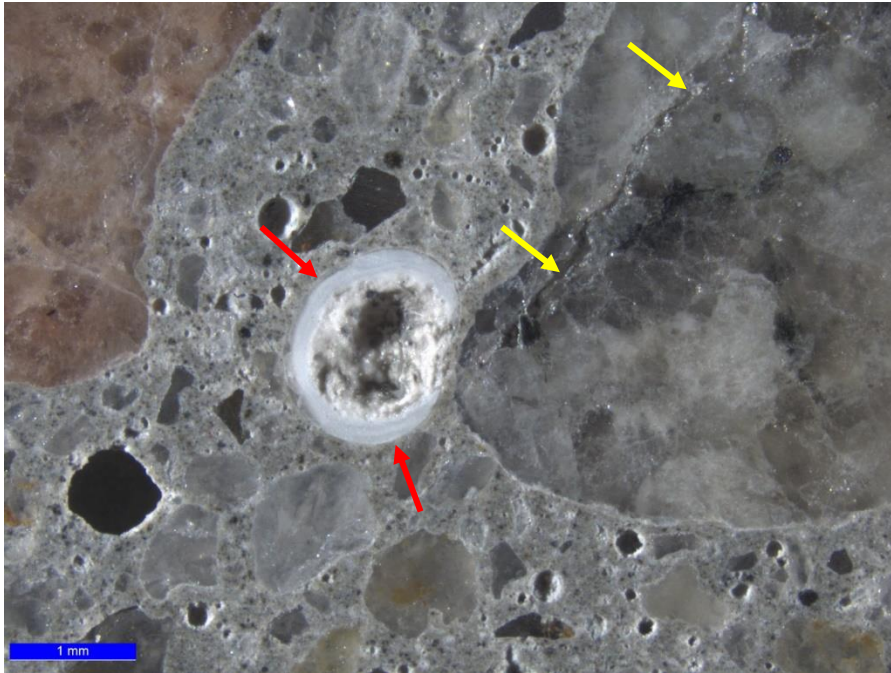
Figure D16. Core 1. ASR gel within an air void (red arrows). The gel likely emanated from the volcanic particle to the right, which contains an internal crack that suggests reactivity (yellow arrows).
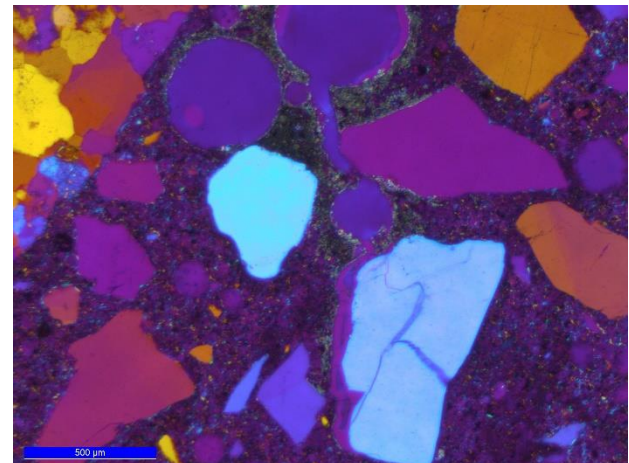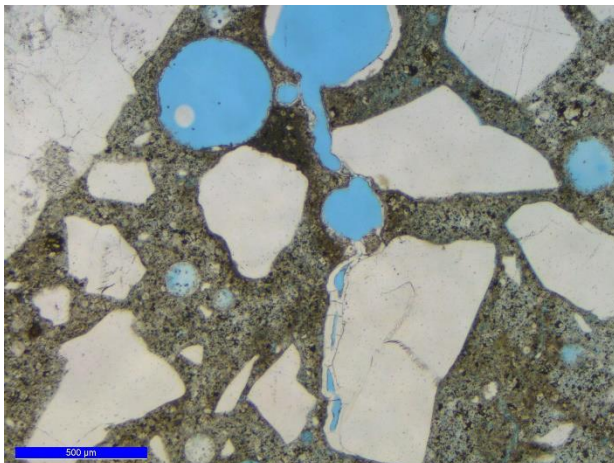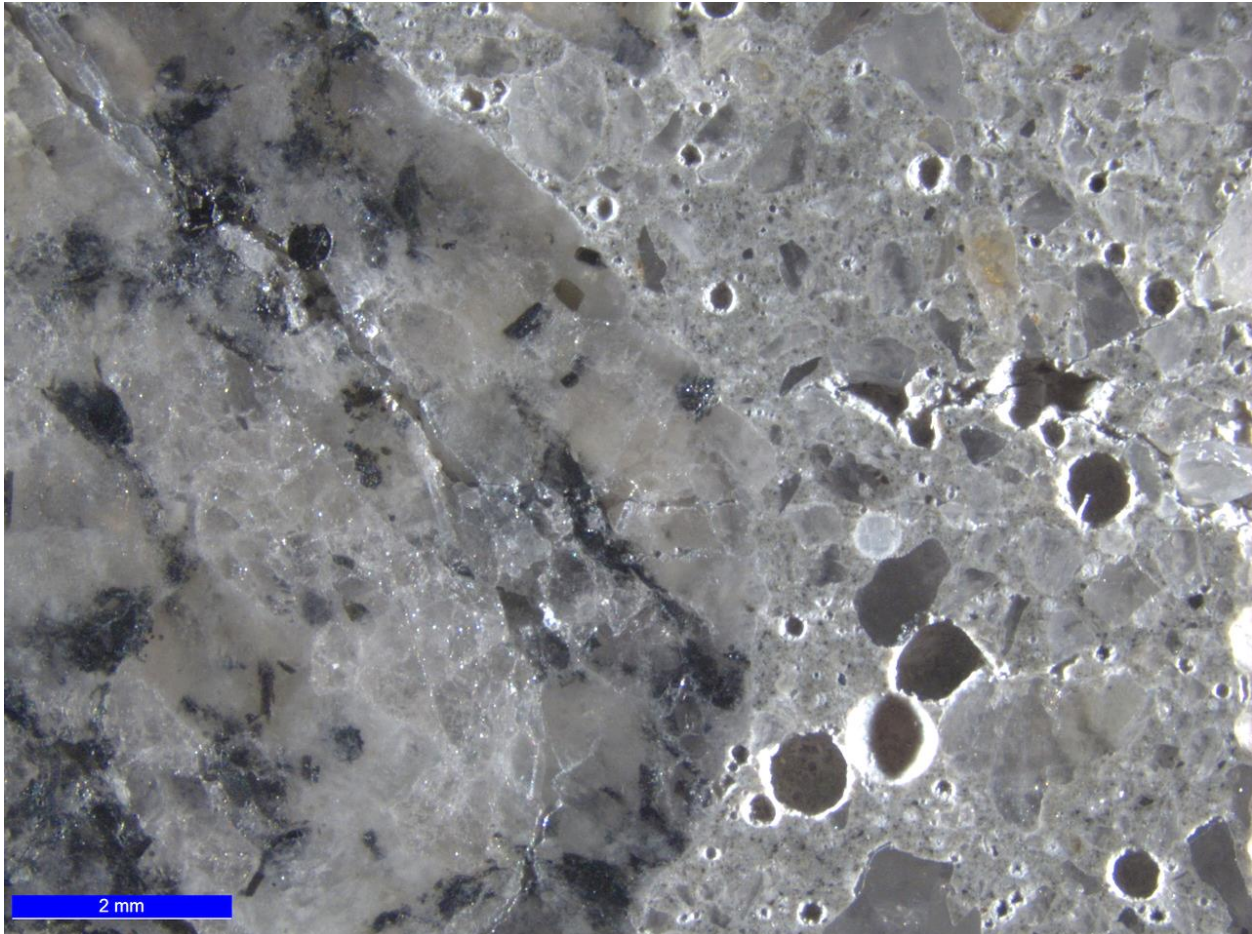
Figure D17. Core 5. Images of ASR gel in air voids and cracks (red arrows) and microcracking (yellow arrows) through and around aggregate particles. The exterior image was taken approximately 3-1/2 inches below the exterior surface, while the photomicrographs were taken 5/8 inch below the surface. Bottom left image taken in plane-polarized light, bottom right image taken in cross-polarized light with a gypsum plate.